Kinetic instability of first order spin waves in ferrite

V. S. Lutovinov, G. A. Melkov, A. Yu. Taranenko, and V. B. Cherepanov

Kiev State University

(Submitted 25 May 1988)
Zh. Eksp. Teor. Fiz. **95**, 760–768 (February 1989)

A kinetic instability of first order spin waves in ferrite is described. This instability is caused by the decay of an intense packet of parametrically excited spin waves. A theory of this instability is developed. The experimental data are in agreement with the conclusions of the theory.

1. INTRODUCTION

Kinetic instabilities in magnetics result from the vanishing of the spin wave damping when the spin-wave spectrum contains regions with a spin wave population differing substantially from a thermodynamically equilibrium population. The case investigated most thoroughly to date is that of second order kinetic instability in ferrite, for which the nonequilibrium is generated by a strong parallel pump.[1,2] Two parametric spin waves (PSW) with frequencies $\omega_p/2$ (ω_p is the pump frequency) and wave vectors $\mathbf{k}_1$ and $\mathbf{k}_2$ generate two secondary spin waves (SW) with wave vectors $\mathbf{k}$ and $\mathbf{k}'$ and frequencies $\omega_{\mathbf{k}}$ amd $\omega_{\mathbf{k}'}$, satisfying the conservation laws

$$\mathbf{k}_1+\mathbf{k}_2=\mathbf{k}+\mathbf{k}', \quad \omega_{\mathbf{k}}+\omega_{\mathbf{k}'}=\omega_p. \tag{1.1}$$

When PSW decays are allowed a first order kinetic instability (KI) may occur, thereby generating secondary spin waves in accordance with the conservation laws

$$\mathbf{k}_p=\mathbf{k}+\mathbf{k}', \quad \omega_p/2=\omega_{\mathbf{k}}+\omega_{\mathbf{k}'}, \tag{1.2}$$

where $\mathbf{k}_p$ is the wave vector of the PSW. The theory of such an instability in a "easy plane"-type antiferromagnetic was developed in Ref. 3 to explain the results of a series of experiments.[4,5] It was demonstrated in Ref. 3 that a kinetic instability develops at pump power levels slightly exceeeding the parametric excitation threshold, and the susceptibility, spectral width of the PSW packet and other characteristics of the nonequilibrium state of the antiferromagnetic beyond the KI threshold were calculated. All these quantities were in reasonable agreement with experimental data[4,5] which provided indirect arguments in favor of the existence of such an instability. However there has been no direct observation of the first order kinetic instability. The difficulty of experimental analysis of this instability can be attributed to the fact that, first, the process (1.2) is possible only in the decaying range of the spectrum, where the influence of nonlinear effects is diminished by strong damping and, second, the secondary spin waves have a short wavelength, which makes it unlikely that they will be radiated from a specimen as electromagnetic oscillations.

The present study is devoted to an investigation of the first order kinetic instability in ferrite. Section 2 develops a theory of KI in ferrite. A nontrivial issue here is the fact that under parallel pumping PSW are near the equator of the resonant surface $\theta_{\mathbf{k}} \approx \pi/2$, although for $\theta_{\mathbf{k}} \approx \pi/2$ the amplitude of the process (1.2) vanishes. The KI threshold is therefore sensitive to the angular structure of the PSW packet. Section 3 describes an experimental technique based on the application of two packets, one of which generates an intense PSW packet, which the other probes the sample at the PSW frequencies. Section 4 provides experimental results indicating the generation of first order kinetic instability at a pump power 6–7 dB over threshold. Section 5 is devoted to a discussion of these results.

2. FIRST ORDER KINETIC INSTABILITY THEORY

We will consider small perturbations $\delta n_{\mathbf{k}}$ of the magnon distribution function in the presence of thermal magons and PSW with the distribution function

$$n_{\mathbf{k}}{}^{p}=\frac{(2\pi)^3(k_p v_p)}{v_0 k_p{}^3} n_p \delta\left(\omega_{\mathbf{k}}-\frac{\omega_p}{2}\right)\delta\left(\theta-\frac{\pi}{2}\right) f(\varphi). \tag{2.1}$$

Here v_p is the group velocity of PSW, v_0 is the elementary cell volume, n_p is the total number of PSW per elementary cell. The function $f(\varphi)$, normalized to unity, describes the distribution of parametric spin waves over the azimuthal angle φ. As demonstrated in Ref. 2, 6 this function is similar to a set of rectangles centered in directions where damping is minimized:

$$f(\varphi)=\frac{1}{2z\Delta\varphi}\begin{cases}1, & |\varphi-\varphi_j|\leqslant\Delta\varphi\\ 0, & |\varphi-\varphi_j|>\Delta\varphi\end{cases}, \tag{2.2}$$

$\varphi_j = 2\pi j/z, j = 1,\ldots, z$. If the magnetic field H is parallel to a fourth order crystallographic axis, then $z = 4$. Experiment has revealed[7] that $\Delta \approx 0.05$–0.01.

The perturbation to the distribution function $\delta n_{\mathbf{k}}$ satisfies the linearized kinetic equation[2]

$$\frac{\partial \delta n_{\mathbf{k}}}{\partial t}+2\gamma_{\mathbf{k}}{}^{0}\delta n_{\mathbf{k}}=\frac{v_0}{\pi^2}\int |V_{\mathbf{k}',\mathbf{k}\mathbf{k}''}|^2 n_{p,\mathbf{k}'}\,\delta(\omega_{\mathbf{k}'}-\omega_{\mathbf{k}}-\omega_{\mathbf{k}''}) \times \delta(\mathbf{k}'-\mathbf{k}-\mathbf{k}'')\,d^3\mathbf{k}'\,d^3\mathbf{k}'', \tag{2.3}$$

where $\gamma_{\mathbf{k}}^0$ is the equilibrium magnon damping, $V_{\mathbf{k}',\mathbf{k}\mathbf{k}''}$ is the three-magnon interaction amplitude:

$$V_{\mathbf{k}',\mathbf{k}\mathbf{k}''}=\frac{\omega_m}{2(2S)^{1/2}}[x_{\mathbf{k}}\exp(i\varphi_{\mathbf{k}})+x_{\mathbf{k}''}\exp(i\varphi_{\mathbf{k}''})], \tag{2.4}$$

$\chi_{\mathbf{k}} \equiv \cos\theta_{\mathbf{k}}$ (here we have taken into account that $\theta_{\mathbf{k}} \approx \pi/2$), S is the magnetic ion spin, $\omega_m = 4\pi g M$, M is the intensity of magnetization, g is the gyromagnetic ratio,

$$\omega_{\mathbf{k}}=\left[\left(\omega_0+\omega_{ex}(ak)^2+\frac{\omega_m}{2}\sin^2\theta_{\mathbf{k}}\right)^2-\frac{\omega_m}{4}\sin^2\theta_{\mathbf{k}}\right]^{1/2}, \tag{2.5}$$

where ω_0 is the gap in the spin wave spectrum, ω_{ex} is the exchange frequency. In our experimental conditions $\theta_{\mathbf{k}}$ is close to $\pi/2$, while the wave vectors of the PSW and SSW are rather large, which allows setting

 0038-5646/89/020432-05$04.00

$$\omega_{\mathbf{k}}=\bar{\omega}+\omega_{ex}(ak)^2-\omega_m x_{\mathbf{k}}^2/2. \tag{2.6}$$

For a spherical specimen

$$\bar{\omega}=\omega_0+\omega_m/2=g(H-{}^4/_3\pi M)+\omega_m/2. \tag{2.7}$$

Equation (2.3) relates the perturbation to the distribution function of magnons with frequency $\omega_{\mathbf{k}}$ to the perturbation of the distribution at frequency $\omega_{\mathbf{k}''}=\omega_p/2-\omega_{\mathbf{k}}$. In the experimental conditions the magnetic field was designed to be close to the thresehold of the process (1.2), H_{3s}, and hence

$$k\approx k'\approx k_p/2, \quad x_{\mathbf{k}}\sim x_{\mathbf{k}''}\ll 1. \tag{2.8}$$

As a result we have

$$({}^1/_2\partial/\partial t+\gamma_{\mathbf{k}}^0)\delta n_{\mathbf{k}}-\Gamma_{\mathbf{k}}(\delta n_{\mathbf{k}}+\delta n_{\mathbf{k}''})=0, \tag{2.9}$$

where

$$\Gamma_{\mathbf{k}}=\frac{\omega_m^2 x_{\mathbf{k}}^2 n_p}{z\Delta f S\{\omega_{ex}a^2k_p^2[(2\omega_m-\omega_{ex}a^2k_p^2)x_{\mathbf{k}}^2+4g\Delta H]\}^{1/2}}, \tag{2.10}$$

$H=H_{3s}-H$, $\gamma_0\equiv\gamma_k^0(k_p/2)$. The KI threshold is achieved when

$$n_p^c=\min_{x_{\mathbf{k}}}\frac{\gamma_0 S\{\omega_{ex}a^2k_p^2[(2\omega_m-\omega_{ex}a^2k_p^2)x_{\mathbf{k}}^2+4g\Delta H]\}^{1/2}}{2\omega_m^2 x_{\mathbf{k}}^2}$$
$$=\frac{\gamma_0 S}{\omega_m}\left(\frac{\omega_{ex}a^2k_p^2}{g\Delta H}\right)^{1/2}\left(1+\frac{\omega_{ex}a^2k_p^2}{2\omega_m}\right)^{1/2}. \tag{2.11}$$

The KI threshold is minimized when

$$x_{\mathbf{k}}=\left(\frac{4g\Delta H}{2\omega_m+\omega_{ex}a^2k_p^2}\right)^{1/2}. \tag{2.12}$$

Equation (2.11) is valid until x_m exceeds the angular width of the PSW packet which is 0.1–0.15 in the experimental conditions[7]. Equation (2.11) can therefore be used when $\Delta H\geqslant\Delta H^*\sim 10$ Oe. When $\Delta H^*\geqslant\Delta H>0$ it is necessary to modify (2.11) by the substitution

$$\Delta H\to\Delta\tilde{H}=\Delta H+\Delta H^*. \tag{2.13}$$

3. EXPERIMENTAL TECHNIQUE

A technique employing two parallel pumps independently acting on a ferrite specimen was employed to investigate the first order kinetic instability. The pump at the higher frequency ω_{p_1} was the primary pump: This pump drove the primary PSW at $\omega_{p_1}/2$, thereby creating a nonequilibrium magnon spectrum and giving rise to a kinetic instability of SSW at frequencies near $\omega_{p_1}/4$. The second pump at ω_{p_2} was the pump, whose purpose was to detect the first pump-driven deviation of the spin wave population N at

$$\omega_{p_2}/2=\omega_{p_1}/4+2\pi\Delta f, \quad 2\pi\Delta f\ll\omega_{p_1}, \ \omega_{p_2}$$

from the thermodynamic equilibrium value N_t. When $N=N_t$ the time until the second pump pulse shuts off t_2^0 (Ref. 8) is determined solely by its supercriticality $p_2=P_2/P_{2\text{th}}$: The ratio of pump P to the pump threshold P_{th}.

If the first pump drives a kinetic instability, we will have $N>N_t$ at frequencies near $\omega_{p_1}/4$, while the time t_2 until the second pulse shuts off begins to diminish: $t_2^*<t_2^0$. This is because the number of spin waves N is the initial number for the second pump-driven parametric instability process that grows exponentially in time. Clearly the greater the initial number the more rapidly this process will cause experimentally detectable changes in the pulse. It is therefore possible to identify the onset of the kinetic instability of spin waves near $\omega_{p_1}/4$ by investigating the time to the trailing edge of the second pump pulse t_2^* when varying the supercritical first pump $p_1=P_1/P_{1\text{th}}$. The time when $t_2^*=f(p_1)$ corresponds, obviously, to the kinetic instability thresehold p_c.

A block diagram of the experimental setup is shown in Fig. 1. The first pump pulse from the magnetron oscillator is fed through a waveguide isolator, precision attenuator PA_1 and a bidirectional coupler to the measurement section containing the ferrite. Attenuator PA_1 was used to regulate the first pump power P_1 reaching the measurement section MS, while the waveguide bidirectional coupler WBC was used to measure the standing wave ratio of the MS and to observe the pulse reflected off the MS. The first pump frequency $\omega_{p_1}=2\pi\cdot 9.4$ GHz, the pulse duration was 100 μs and the pulse repetition rate was 10 Hz. The MS took the form of a hollow cavity constructed from a standard 3-cm waveguide producing TE_{012} modes at the first pump frequency.

An open dielectric cavity whose lowest magnetic mode was tuned to resonance to the second pump frequency ω_{p_2} was installed near the end wall of the hollow waveguide cavity (see Fig. 1). An aperture of diameter 2 mm was drilled in the dielectric cavity to provide a mount for a ferroyttrium garnet monocrystalline sphere of diameter 1.5 mm with a ferromagnetic resonance linewidth of 0.33 Oe. The sphere rotated freely within the aperture and the easy axis of magnetization [111] of the sphere was oriented along the constant magnetic field **H**. A wire loop was used to couple the dielectric cavity to the coaxial second pump line. At the ferrite mount point the oscillatory magnetic fields of both

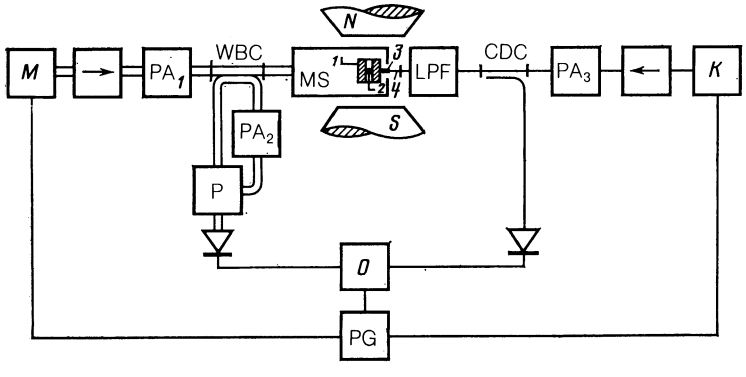

FIG. 1. Block diagram of experimental setup: *M*—magnetron oscillator, *K*—klystron generator, PA—precision attenuator, CDC—coaxial directional coupler, WBC—waveguide bidirectional coupler, MS—measurement section containing open dielectric cavity (1), ferrite (2) and coupling element (3) for coupling the dielectric cavity to the coaxial line (4), LPF—low-pass filter, PG—pulse generator, O—oscillograph.

pumps were parallel both to one another and to the direction of the constant magnetic field **H**.

The second pump signal was injected to the dielectric cavity from the klystron generator through the microwave isolator, precision attenuator PA_3, the coaxial directional coupler CDC, the low-pass filter LPF and the loop coupling element. Attenuator PA_3 controlled the second pump power P_2, and the coulper CDC was used to determine the waveform of the second pump signal reflected off the measurement section, while the low-pass filter was used to block the first pump signal from reaching the second pump coaxial section. The second pump was blocked from the first pump waveguide section by virtue of the dimensions of the waveguides in this section which were subcritical relative to the second pump frequency. The second punp frequency was tunable over 4685–4785 MHz, allowing frequency detuning of $\Delta f = (1/2\pi)\cdot(\omega_{p_2}/2 - \omega_{p_1}/4)$ in the range -7.5–42.5 MHz. The duration and repetition rate of the klystron generator pulses matched those of the magnetron pulses. Initiation of the klystron generator pulse was delayed by $\tau = 0$–1 μs with respect to the end of the magnetron pulse.

The threshold powers for the onset of spin wave instabilities $P_{1\text{th}}$ and $P_{2\text{th}}$ were identified by the appearance of the trailing edge[8] on the first and second pump pulses reflected off the MS, respectively. The experiments were carried out at room temperature.

4. EXPERIMENTAL RESULTS

In the first series of experiments we initially injected a 100-μs first primary pump pulse at a higher frequency ω_{p_1}. The second pulse—the probe pump—was then injected and the first pulse was simultaneously switched off. The dependence of the time to the trailing edge of the second pump pulse t_2* on the subcritical first pump p_1 is shown in Fig. 2. It is clear that when $p_1 > p_c \approx 7$ dB there is a sharp jump in this relation towards smaller t_2*. This indicates an increase in the number of spin waves N at frequency $\omega_{p_2}/2 = \omega_{p_1}/4 + 2\pi\Delta f$ when $p > p_c$ (in Fig. 2 $\Delta f = -3$ MHz).

The first pump power will also influence the time to the trailing edge of the second pump pulse t_2* in a limited range of constant magnetic fields $H = 590$–650 Oe (see Fig. 3). The upper bound corresponds to the three-magnon splitting field H_{3s}^{9} of the primary PSW, while the lower bound corresponds to the saturation field H_s of the specimen. Within this range the kinetic instability threshold p_c changes insignificantly, from ≈ 6 dB in weak fields to ≈ 7 dB in strong fields. The influence of the first pump power on t_2* (see Fig. 2) largely depends on the constant magnetic field magnitude H. With diminishing H it will first arise when $H = 650$ Oe, and will then rapidly (when $H = 646$ Oe) reach a maximum and will then diminish. If t_2* goes from 20 to 8 μs when $H = 646$ Oe ae indicated by Fig. 2, when $H = 623$ Oe and with all other conditions remaining the same the time t_2* will only drop from 20 μs to 18 μs.

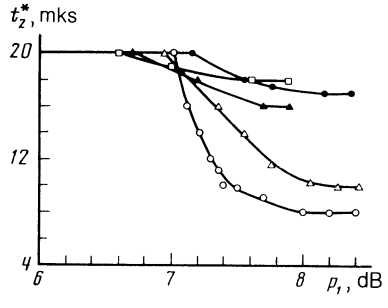

FIG. 2. Time t_2* to onset of shear in second pump pulse for $p_2 = 0.4$ dB plotted as a function of the supercritical first pump p_1 at $\tau = 0$: ●—$H = 650$ Oe, ○—646 Oe, △—644 Oe, ▲—630 Oe, □—623 Oe.

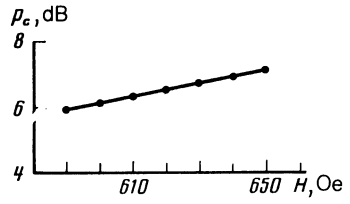

FIG. 3. The threshold supercriticality p_c of the first order kinetic instability p_c plotted as a function of the constant magnetic field H.

Figure 4 plots the threshold of the spin wave kinetic instability as a function of the frequency detuning Δf relative to $\omega_{p_1}/4$. It is clear that spin waves of frequency $\omega_{p_1}/4$ have a minimum threshold $p_{c\,\min} = 6.7$ dB. With increasing subcriticality the frequency range of the kinetic instability broadens noticeably. It reaches 33 MHz as early as $p = p_{c\,\min} + 0.8$ dB.

Increasing the second pump pulse delay reduced the influence of the first pump on t_2*. Figure 5 clearly indicates that even in the case of maximum influence ($H = 646$ Oe) it is virtually absent when $\tau = 0.15$ μs. The influence of the first pump will vanish even more rapidly with diminished H For example, at $H = 644$ Oe it was observed until $\tau \leqslant 0.1$ μs.

The behavior of the nonlinear susceptibility χ of the ferrite with respect to the first pump was carefully analyzed for $p > p_c$. No features in the behavior of $\chi(H)$ and $\chi(p)$ were observed near $p \approx p_c$, to an accurancy of $\Delta\chi/\chi \sim 10^{-2}$. No radiation from the ferrite for $p > p_c$ at $\omega_{p_1}/2$ and $\omega_{p_1}/4$ was detected. The radiation was recorded through the second pump circuit; sensitivity of the setup was 10^{-11} W.

The effects that occur from the simultaneous activation of two pumps of identical duration (100 μs) analogous to the setup used in Ref. 10 to investigate second order KI were also analyzed. It was found that the first pump power at $p_1 p_c$ substantially reduces (rather than increases as suggested in Ref. 10) the second pump-driven parametric excitation threshold of the spin waves $P_{2\text{th}}$: Fig. 6 indicates that when $p_1 = p_c + 1.15$ dB this reduction ~ 2 dB. When $p_1 < p_c$ the first pump does not influence the second pump. And here again unlike Ref. 10 the second pump does not diminish but rather increases the KI threshold after the parametric insta-

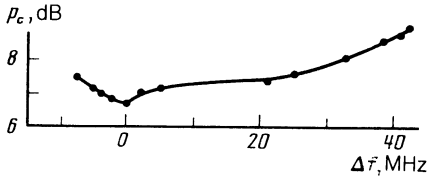

FIG. 4. The threshold supercriticality p_c of the first order KI plotted as a function of detuning Δf relative to the frequency $\omega_{p_1}/4$; $\tau = 0$, $H = 646$ Oe.

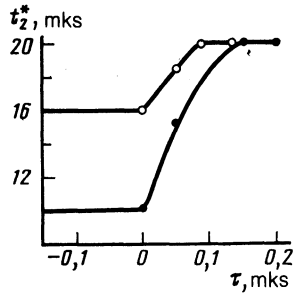

FIG. 5. Time t_2* to onset of shear in second pump pulse plotted against delay τ: ●—H 646 Oe, ○—644 Oe; p_1–p_c. = 0.4 dB.

bility threshold $P_2 > P_{2th}$ (Fig. 7). This threshold is also determined based on the reduction in the time to the trailing edge of the second pump pulse from increasing power of the first pump t_2*. The KI threshold is identical for both simultaneous and successive action of the two pumps as $P_2 \to P_{2th}$. However when both pumps operate simultaneously the influence of the first pump on time t_2* varies little with diminishing magnetic field, unlike the cause of successive pumps. This fact it possible to improve the accuracy of KI threshold measurements in the case of simultaneous pumps, particularly in weak fields. The experimental data shown in Fig. 3 for $H < 620$ Oe were therefore obtained in an experiment with simultaneous pumps, while the case $H > 620$ Oe were obtained with successive pumps at $\tau = 0$.

When the leading edge of the second pump pulse is delayed with respect to the leading edge of the first pump pulse, the influence of the second pump power on the KI threshold diminishes and vanishes when the trailing edge of the second pump pulse falls outside the range of the first pulse.

5. DISCUSSION OF RESULTS

The experimentally observed threshold drop in the time to t_2* to the trailing edge of probe pump pulse of frequency ω_{p_2} as the supercriticality of the primary pump of frequency ω_{p_1} can be attributed to the threshold increase in the number of spin waves with frequencies near $\omega_{p_2}/2$ (SSW) resulting from the kinetic instability of these spin waves. The reduction in time t_2* could also be attributed to other causes, such as diminishing SSW damping due to their interaction with PSW below the KI threshold. However according to (2.10) this drop is proportional to n_p and does not manifest a threshold character. One additional aspect suggesting that t_2* diminishes as a result of KI is the fact that this reduction

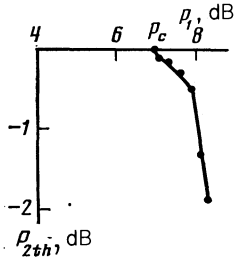

FIG. 6. Second pump threshold P_{2th} plotted as a function of the supercriticality p_1 of the first pump for simultaneous pump action; H = 646 Oe; 0 dB along the vertical axis corresponds to p_{2th} in the absence of the first pump ($p_1 = 0$).

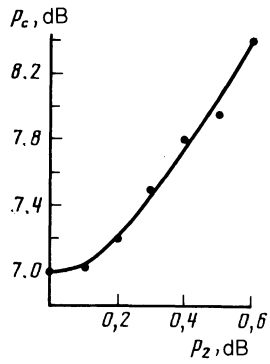

FIG. 7. The threshold supercriticality p_c of the first order KI plotted as a function of the supercriticality p_2 of the second pump for simultaneous pump action; H = 646 Oe.

occurs only in the magnetic field range $H_s \leqslant H \leqslant H_{3s}$, i.e., where processes (1.2) leading to KI are allowed.

The experimental data make it possible to estimate the threshold number of PSW n_p^c at which KI ensues. Indeed nonlinear damping[9] is the fundamental PSW energy dissipation mechanism in the magnetic field range $H_s \leqslant H \leqslant H_{3s}$. The imaginary part of the susceptibility in this case takes the form[2]

$$\chi'' = \frac{2\gamma_p n_p}{|hV|^2} = \chi_m'' \frac{p^{1/2}-1}{p^{1/2}}, \qquad (5.1)$$

where V is the PSW-to-pump coupling coefficient, h is the pump field amplitude, and χ_m'' is the maximum value of the imaginary part of the nonlinear susceptibility for longitudinal pumping in the case of nonlinear damping.[2] The threshold number of PSW is then easily estimated

$$(n_p^c)_{\exp} = \frac{\gamma_1 \omega_{p1}}{\omega_m^2} \frac{S}{2} 4\pi\chi_m'' \frac{\chi_c''}{\chi_m''-\chi_c''}, \qquad (5.2)$$

where χ_c'' is the imaginary part of the susceptibility at the KI threshold. This should be compared to the theoretical prediction (2.11). Unfortunately γ_0, $\Delta\varphi$ and $\Delta H = \Delta\tilde{H} + \Delta H$* are not known with sufficient accuracy. However we know that $\gamma_0 \leqslant \gamma_1$, $\gamma_1/\omega_m \approx 1.7 \cdot 10^{-4}$, while the angular dimensions of the PSW packet $\bar{x} \sim (g\Delta H^*/\omega_m)^{1/2} \sim 0.1$, $\Delta\varphi \sim 0.1$. Setting $\gamma_0/\omega_m = 1.5 \cdot 10^{-4}$ from (5.2) and (2.11) we obtained the threshold PSW numbers for several characteristic magnetic fields:

H, Oe	650	640	610	590
$(n_p^c)_{\exp} \cdot 10^4$	5.3	5.1	4.0	3.4
$n_p^c \cdot 10^4$	2.2	1.8	1.2	1.1

The PSW threshold numbers n_p^c determined from experimental results and from (2.11) therefore agree to within an order of magnitude and have an identical magnetic field dependence across the entire magnetic field range $H_s \leqslant H \leqslant H_{3s}$. The discrepancy by a factor of three in these quantities is most likely related to the rough estimate of the unknown parameters entering into the expression (2.11) for the threshold.

The increase in the frequency range over which KI develops as a function of the power of the first pump, described in Sec. 4, has a simple qualitative explanation. The angular width of the PSW packet at $\omega_{p_1}/2$ does in fact grow with increasing pump power which, consistent with the conserva-

tion laws (1.2) for magnons with spectrum (2.5), may excite secondary magnons with the wave vectors deviating substantially from the equator (and with a corresponding large value of $|\theta_k - \pi/2|$) over a broader frequency range as well. It is necessary to know the angular distribution of the PSW in order to carry out a quantitative analysis of the dependence of the KI threshold on the frequency detuning Δf.

The increase in the time t_2^* to the trailing edge as a function of the delay between pulses (see Fig. 5) can, obviously, be attributed to the relaxation of the start number of the waves $N(0) \propto \exp(-2\gamma_0\tau)$.

In order to interpret the behavior of susceptibility beyond the KI threshold it is necessary to investigate the instability-limiting mechanisms accounting for the inverse influence of SSW on PSW analogous to the process employed for an antiferromagnetic.[3] Evidently the most effective SSW energy dissipation mechanism in ferrite is merging with PSW which, as demonstrated in Ref. 3, causes a minor change in the susceptibility near the KI threshold and causes renormalization of the nonlinear damping coefficient far beyond threshold. The behavior of the susceptibility observed experimentally is therefore in argeement with qualitative concepts regarding the superthreshold behavior of nonequilibrium magnons.

Results from experiments carried out when two pumps are activated simultaneously can also be explained qualitatively within the framework of first-order KI theory. Indeed the PSW at $\omega_{p_1}/2$ (PSW_1) will, consistent with (2.8) partially cancel damping of magnons at $\omega_{p_2}/2$, and the greater the number of PSW_1, the lower the parametric instability threshold for the second pump. If the second pump power exceeds the parametric excitation threshold, the resulting PSWs at $\omega_{p_2}/2$ (PSW_2) magnify the damping of magnons at $\omega_{p_1}/2$, causing the number of PSW_1 to drop. It is important to mention that the quasielastic scattering processes of PSW_1 and PSW_2 are linked by relatively weak four-magnon interactions and cannot play any substantial role in the development of first order KI.

The experimental data set therefore allow us to conclude that first order KI ensues in the field range $H_s \leqslant H \leqslant H_{3s}$ when the parametric excitation threshold is exceeded by 6–7 dB.

[1]A. V. Lavrinenko, V. S. L'vov, G. A. Melkov and V. B. Cherepanov, Zh. Eksp. Teor. Fiz. **81**, 1022 (1981) [Sov. Phys. JETP **81**, 542 (1981)].
[2]V. S. L'vov, *Nelineynye spinovye volny* (*Nonlinear Spin Waves*), Nauka, Moscow, (1987) Sections 21, 54, 56.
[3]V. S. Lutovinov, G. E. Fal'kovich and V. B. Cherepanov, Zh. Eksp. Teor. Fiz. **90**, 1781 (1986) [Sov. Phys. JETP **90**, 1045 (1986)].
[4]B. Ya. Kotyuzhanskiy and L. A. Prozorova, Zh. Eksp. Teor. Fiz. **81**, 1913 (1981) [Sov. Phys. JETP **81**, 1013 (1983)]; Zh. Eksp. Teor. Fiz. **83**, 1567 (1982) [Sov. Phys. JETP **83**, 903 (1982)]; Zh. Eksp. Teor. Fiz. **86**, 658 (1984) [Sov. Phys. JETP **86**, 384 (1984)].
[5]B. Ya. Kotyuzhanskiy, L. A. Prozorova and L. E. Svistov, Zh. Eksp. Teor. Fiz. **86**, 1101 (1984) [Sov. Phys. JETP **86**, 644 (1984)].
[6]V. S. L'vov and V. B. Cherepanov, Zh. Eksp. Teor. Fiz. **76**, 2266 (1979) [Sov. Phys. JETP **76**, 1145 (1979)].
[7]A. S. Bakay, I. V. Krutsenko, G. A. Melkov and G. G. Sergeeva, Zh. Eksp. Teor. Fiz. **76**, 231 (1979) [Sov. Phys. JETP **76**, 118 (1979)].
[8]E. Schlömann, I. I. Green and V. J. Milano, J. Appl. Phys. **31**, 386S (1960).

Translated by Kevin S. Hendzel